Content Aware Image Pre-Compensation

Jinwei Ye, *Member, IEEE,* Yu Ji, *Member, IEEE,* Mingyuan Zhou, *Student Member, IEEE*
Sing Bing Kang, *Fellow, IEEE* and Jingyi Yu, *Member, IEEE*

Abstract—The goal of image pre-compensation is to process an image such that after being convolved with a known kernel, will appear close to the sharp reference image. In a practical setting, the pre-compensated image has significantly higher dynamic range than the latent image. As a result, some form of tone mapping is needed. In this paper, we show how global tone mapping functions affect contrast and ringing in image pre-compensation. We further enhance contrast and reduce ringing by considering the visual saliency. Specifically, we prioritize contrast preservation in salient regions while tolerating more blurriness elsewhere. For quantitative analysis, we design new metrics to measure the contrast of an image with ringing. Specifically, we set out to find its "equivalent ringing-free" image that matches its intensity histogram and uses its contrast as the measure. We illustrate our approach on projector defocus compensation and visual acuity enhancement. Compared with the state-of-the-art, our approach significantly improves the contrast. We also perform user studies to demonstrate that our method can effectively improve the viewing experience for users with impaired vision.

Index Terms—Image Deconvolution, Pre-Compensation, High Contrast, Ringing-Free, Non-Linear Tone Mapping, Saliency

✦

1 INTRODUCTION

ALL projectors introduce some form of visual blurring due to its optics and possibly non-planar projection surface. One way to reduce this problem is to first characterize its blur (defocus) kernel and preprocess the image such that the resulting projected image is sharp. The preprocessing step is called *image pre-compensation*.

More generally, image pre-compensation is a long standing problem in image processing with numerous applications in computer vision and graphics. Given a sharp reference image I and the blur kernel or point spread function (PSF) K, the goal is to find a "pre-compensated" image J which, after being convolved with K, will appear close to I. In the projection defocus compensation example above, by projecting J, the actual perceived image should appear nearly focused.

Pre-compensation vs. Deblurring. At first glance, image pre-compensation may resemble image deblurring as both can be viewed as "deconvolution". The two problems, however, are inherently different. In image deblurring, there *always* exist some "ground truth" J to produce I under kernel K. The ill-posedness of deblurring rises from the invertibility of K, *i.e.*, if K is not invertible, there exist multiple J that can produce the same I. To resolve this ambiguity, classical Wiener filter [1] uses regularization to enforce invertibility whereas more advanced solutions add priors such as gradient sparsity [2], [3], [4], [5], edge sharpness [6], [7], [8] or new irradiance-based blur model [9] to constrain the solution.

In image pre-compensation, there usually does *not* exist any valid solution J. In projector defocus compensation for example,

---

- *Jinwei Ye and Yu Ji contributes equally to this work.*
- *Jinwei Ye is now with the Division of Computer Science and Engineering, Louisiana State University, Baton Rouge, LA 70803*
  E-mail: jye@csc.lsu.edu
- *Yu Ji is now with Plex VR.*
- *Mingyuan Zhou is a graduate student in the University of Delaware.*
- *Sing Bing Kang is with Microsoft Research, Redmond.*
- *Jingyi Yu is with University of Delaware and Shanghai Tech University.*

the convolution kernel is a low pass filter that removes the high frequency components of J. J is expected to preserve sharpness even after being blurred. Therefore, the problem is ill-posed in that no "ground truth" solution exists.

Dynamic Range Problem. A serious problem in image pre-compensation is the significant increase in dynamic range. Assume K is invertible, conceptually J can be directly computed as

$$J = I \otimes K^{-1} \qquad (1)$$

where $\otimes$ denotes convolution. Consider a randomly generated 1D invertible kernel and a 1D image of a step edge $[0, 1]$[1]. The resulting J has range $[-2.9, 4.9]$, as shown in Fig. 1. In the projector defocus compensation case, we will need to use J as the input to the projector and therefore we will have to first compress the rang (tone map) J to $[0, 1]$.

The simplest tone mapping function is linear range compression. In the simple 1D example above, if we apply linear tone mapping on J as $l(J)$, the resulting $I = l(J) \otimes K$ will have dynamic range $[0.4, 0.6]$, much narrower than its original one $[0, 1]$, as shown in Fig. 1. In the projector defocus case, it will lead to severe contrast loss. More sophisticated tone mapping such as power function slightly broadens the dynamic range and contrast of I but at the same time introduces ringing. Most previous approaches assume relatively small kernels K and resort to optimization schemes such as steepest descent [10] and Wiener filters [11], [12]. However, these techniques are less effective on larger kernels. By far, only a handful of techniques address the role of tone mapping functions in image deconvolution/deblurring [9], [13], [14] while the analysis in image pre-compensation is largely missing.

We believe our paper is the first to systematically study how the tone mapping function affects ringing and contrast in image pre-compensation. In this work, we focus on *global* tone mapping functions. We first show that linear tone mapping completely eliminates ringing but incurs severe contrast loss. In contrast,

---

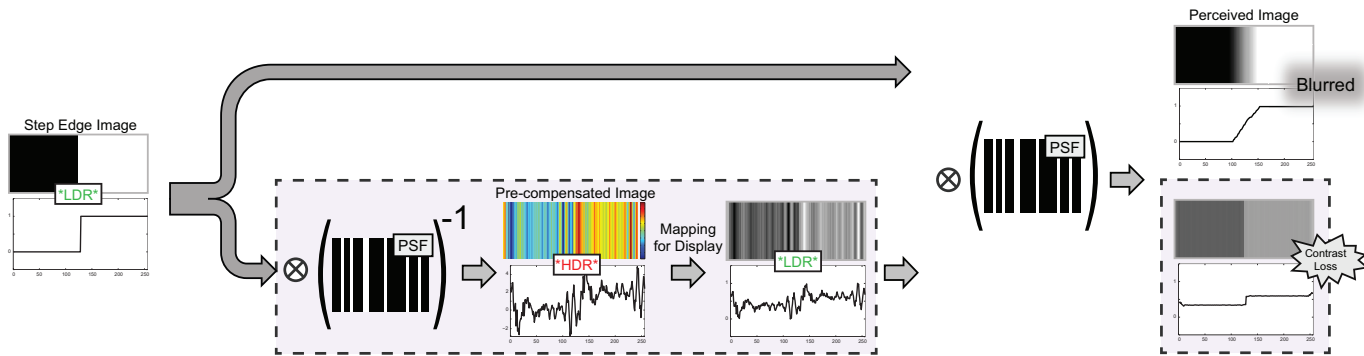1. In this paper, we assume the display's dynamic range is [0, 1]

Fig. 1. Effect of simple linear pre-compensation. The PSF can be from a typical projector, with the input image being of LDR (low dynamic range). Top row: With no pre-compensation, the step edge image is blurred. Bottow row: The pre-compensated image of a step edge under an invertible kernel incurs a significant increase in dynamic range (HDR, or high dynamic range). Linear tone mapping produces a ringing-free sharp result but significantly reduces the scale (contrast) of the step.

non-linear tone mapping functions such as power curves slightly enhances contrast but introduces ringing. To conduct a quantitative analysis, we design new metrics to measure the contrast of an image with ringing. Specifically, we set out to find its "equivalent ringing-free" image that matches the intensity histogram and uses its contrast as the measure. Our approach hence enables reliable comparisons between different tone mapping functions as well as effective constructions of specific tone mapping functions to achieve a target contrast.

We demonstrate our technique on two important applications: projector refocusing and visual acuity enhancement. For projector defocusing, we show that our technique outperforms the state-of-the-art solutions based on steepest descent [10] and Wiener filters [11], [12] on large kernels. For visual acuity enhancement, our technique can improve the visual experience for people with myopia or hyperopia when not wearing corrective lenses. Specifically, we provide a simple user interface to trade-off between ringing and contrast; this interface allows the user to adjust the amount of ringing for generating the optimal curve. Our user study shows that our technique is effective and comparable to the state-of-the-art solutions [15], [16] in both visual quality and quantitative measures.

This work extends our previous publication [17]; there is significant improvement in algorithm design. Visual saliency is used to customize the tone mapping function. More specifically, contrast loss is weighted more heavily in salient for estimating the optimal tone mapping function. This results in salient regions having higher contrast and less ringing while the rest of the image may be compromised by some blurriness. User studies show preference for results of our technique over those of competing state-of-the-art techniques.

The remainder of the paper is organized as follows: We first review related work in Section 2. We define the tone mapping problem in image pre-compensation in Section 3 and show how we optimize the tone mapping function in Section 4. Content-aware pre-compensation is described in Section 5. Experiments and evaluations are shown in Section 5. We suggest areas for future work in Section 6.

2 RELATED WORK

In this section, we briefly review previous state-of-the-art techniques related to image pre-compensation.

Image Deconvolution. Image pre-compensation is closely related to the image deconvolution problem because both involve kernel inversion. Image deconvolution is widely used in image restoration for removing blur [2], [3], [18] and/or noise [19], [20]. Classical algorithms include the Richardson-Lucy method [21] and Wiener deconvolution [1]. Richardson-Lucy [21] models image noise as a Poisson distribution. Wiener deconvolution [1] imposes the Gaussian assumption for both noise and image gradients in order to enforce kernel invertibility. Priors such as gradient sparsity [2], [3], [4], [5], edge sharpness [6], [7], [8] or irradiance-based blur model [9] have been used to constrain the deconvolution problem. More recently, Xu et al. [22] propose a deep convolutional neural network for image deconvolution.

Image deconvolution has also been used for improving the visual acuity for users with vision impairment. For example, Alonso et al. [15], [23] use the classical Wiener deconvolution to compute the pre-compensated image for display on a computer screen and discuss how contrast loss affects the user experience. They further improve the viewing experience through edge enhancement [24]. More recently, Montalto et al. [25] use constrained total variation to pre-correct images for observers with visual aberrations. Although these approaches are able to produce sharper images for vision impaired viewer, such images suffer from significant contrast loss (especially when the viewer's visual aberration is severe). By comparison, our method balances contrast and ringing in estimating the pre-compensated image.

Projector Compensation. Projector compensation is an important application to image pre-compensation and has been heavily studied to improve projection quality. There are techniques that use photometric compensation (e.g., [26], [27]) or geometric compensation (e.g., [28]). The seminal works of Zhang and Nayar [10] and Brown et al. [11] are the first to compensate defocus blurs using image pre-compensation. Brown et al. [11] and Oyamada and Saito [12] use Wiener filters whereas Grosse et al. [29] use a coded aperture to improve PSF invertibility. Their techniques work well for small kernels where the dynamic range of the pre-compensated image is about the same as the reference image. Zhang and Nayar [10] bypassed the tone mapping process through constrained iterative steepest descent. At each iteration, they clamp the latest estimation to $[0, 1]$. For larger kernels, the optimized results neither guarantee good contrast or ringing suppression. In this work, we systematically study the relationship between contrast and ringing in image pre-compensation and propose to

strike a balance by non-linear tone mapping.

Computational Displays. There are also hardware solutions for compensating for the visual blurriness, namely through the use of computational displays/projectors. A comprehensive survey on customized computational devices is provided in [30]. The systems of [16], [31], [32] are most related to blur compensation. Pamplona *et al.* [31] design a special computational display using multiple LCD layers. Their method effectively enhance the contrast of pre-compensated images. However, their device cannot display color images and the field-of-view is very limited. Huang *et al.* [16], [32] develop a multilayer pre-filtering on a ultra-high dynamic range light field display to enhance contrast. All these solutions use simple tone mapping functions and rely on the displays themselves to enhance contrast. By comparison, our approach is a software content-adaptive approach that improves the visual quality of pre-compensated image through a global non-linear tone mapping function.

3 TONE MAPPING IN IMAGE PRE-COMPENSATION

We first study how tone mapping affects the dynamic range, contrast, and ringing in image pre-compensation. The phenomena of significant dynamic range stretch in image deconvolution has been widely documented in signal processing [33] and computer graphics/vision literature [10], [15], [16], [32]. Briefly, the stretch is due to matrix inversion.

Recall that the convolution kernel K can be written in form of a Toeplitz matrix with block-circulant-with-circulant-block (BCCB) structure which can be diagonalized by singular value decomposition (SVD) as $K = U\Lambda V^*$, where U and V are the left and right singular vectors and Λ is a diagonal matrix composed of the square roots of eigen values. Let $\lambda_{\min}$ be the minimum eigen value in Λ. Since the eigen values of K^{-1} are the reciprocal of K's, the maximum in Λ' is then $\lambda'_{\max} = 1/\lambda_{\min}$. If $\lambda_{\min}$ is close to zero, $\lambda'_{\max}$ can be very large, resulting range expansion in J. This implies that J can be of a much higher dynamic range (HDR) and therefore cannot be "physically" implemented, *e.g.*, used as an input to the projector. The question is then how to map dynamic range of J to $[0, 1]$ (normalized version of the usual range $[0, 255]$).

We first define our notations. Assume the sharp reference image I has range $[0, 1]$ and the computed J has range $[min(J), max(J)]$. Given a tone mapping function $f : [min(J), max(J)] \mapsto [0, 1]$, we map J to J_f as the final pre-compensated image and denote the resulting convolution result as $I_f = J_f \otimes K = f(J) \otimes K$. An ideal f should produce $I_f \approx I$. We summarize our notations in Table 1.

3.1 Linear Mapping: The Baseline Performance

As shown in the example of Fig. 1, the simplest f is the linear compression function l:

$$J_l = l(J) = \frac{J - min(J)}{r}, \qquad (2)$$

where $r = max(J) - min(J)$, *i.e.*, the span of the dynamic range. Convolving J_l with K, we have I_l as

$$I_l = l(J) \otimes K = \frac{(I - \mu)}{r}, \qquad (3)$$

where $\mu = min(J) \otimes K$ is a constant. I_l is a shifted and scaled version of I, and therefore should *not* contain any ringing effect. However, it suffers from significant contrast loss.

TABLE 1
Table of Notations

Symbol	Description
I	Reference sharp image
K	Blur kernel
J	Pre-compenstated image before tone mapping
l	Linear compression function
s	Our proposed "s" shaped mapping function
f	General tone mapping function
J_f	Tone mapped pre-compensated image ($J_f = f(J)$)
I_f	Tone mapped restored sharp image ($I_f = f(J) \otimes K$)
m	Slope of a linear tone mapping function
r	Dynamic range span
c	Image contrast
ζ	Contrast factor
H	Image histogram
I_{RF}	Equivalent ringing free image
Γ	Ringing measurement

For a ringing-free image I, we can define its contrast by root mean square (RMS) as:

$$c(I) = \sqrt{\frac{1}{n} \sum_{i=1}^{n} (I(i) - \bar{I})^2}, \qquad (4)$$

where n is number of pixels and $\bar{I}$ is the average intensity value.

Since I_l is ringing free, we can compute its *contrast factor* ζ with respect to I as $\zeta(I_l) = c(I_l)/c(I) = 1/r$. Notice that if I is of uniform intensity, $c(I) = c(I_f) = 0$. In this singular case, we define $\zeta(I_f) = 1$, indicating no contrast lost. Notice that r can be very large even with a moderate size K. For example, in an extreme case from the BSDS500 [34] dataset, a 5×5 Gaussian kernel of $\sigma = 2.5$ (here we assume J can be obtained by Wiener filter) results in $r = 17$, *i.e.*, the contrast loss is significant ($\zeta = 1/17$). In this paper, we use J_l as the baseline result and compare it with other tone mapping functions.

3.2 General Tone Mapping

For a general tone mapping function, we assume it is constructed by composing an additional tone mapping function $f : [0, 1] \mapsto [0, 1]$ onto the baseline result J_l. This significantly simplifies our analysis. For example, many classical tone mapping functions such as Gamma curves can be directly modeled using f. The final tone mapping function hence is $f \circ l = f(l(J)) = f(J_l)$ and we denote J_f as the pre-compensated result and I_f the perceived image.

General Linear Mapping. Let us first consider the general linear mapping with truncation:

$$J_f = \begin{cases} 0, & 0 \leq J_l < -\frac{b}{m} \\ mJ_l + b, & -\frac{b}{m} \leq J_l \leq \frac{1-b}{m} \\ 1, & \frac{1-b}{m} < J_l \leq 1 \end{cases} \qquad (5)$$

When no truncation occurs, we have

$$I_f = (mJ_l + b) \otimes K = mI_l + \delta \qquad (6)$$

where $\delta = b \otimes K$ is a constant. Similar to the baseline case, I_f is also ringing-free and its contrast factor is

$$\zeta(I_f) = \frac{c(I_f)}{c(I)} = \frac{c(I_f)}{r \cdot c(I_l)} = \frac{m}{r} \qquad (7)$$

$m = 1$ corresponds to the baseline function l. If $m < 1$, $c(I_f) < c(I_l)$, *i.e.*, we will lose more contrast. If $m > 1$, $c(I_f) > c(I_l)$,
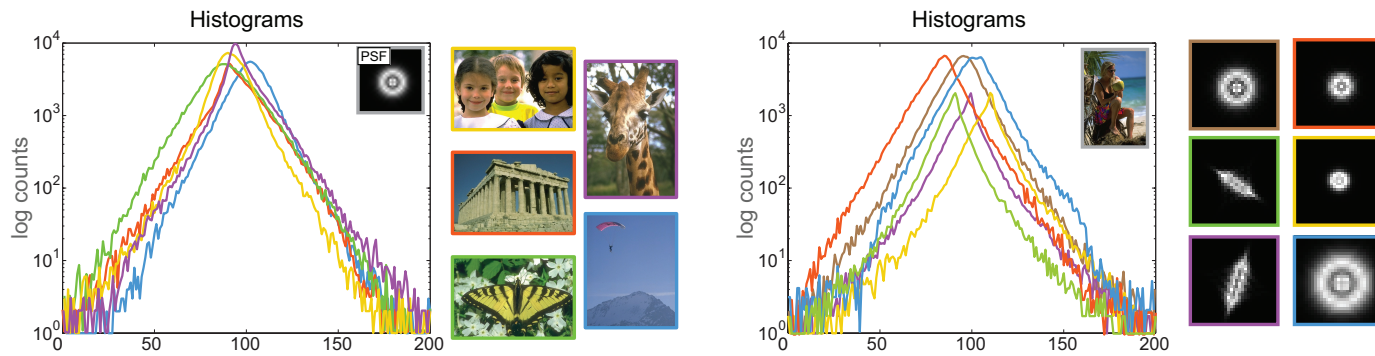
Fig. 2. Histograms of pre-compensated natural images. (a) Histograms of five natural images from BSDS500 [34] pre-compensated by one invertible kernel. (b) Histograms of one natural image pre-compensated using six different kernels. Notice that the histogram changes more dramatically over different kernels than over different images.

we will gain contrast. However, when $m > 1$, many pixels in J_f will saturate and need to be clamped to 0 or 1. As a result, although the contrast is enhanced, I_f will be contaminated by clamping. We denote the general linear mapping without truncation as f_m (m is the slope) and we will use it to model the contrast on ringing-corrupted images.

Non-linear Mapping and Ringing. When f is non-linear, I_f will induce ringing. The cause of ringing can be explained in the frequency domain. Assume the PSF K at a specific frequency ω_n is a_n. Therefore, the corresponding coefficient of K^{-1} at frequency ω_n is $1/a_n$. Let I be a step edge function and its corresponding Fourier coefficient at ω_n is v/n for $n \neq 0$, where v is some constant. By Eqn. 1, the coefficient of J at frequency ω_n is $v/n \cdot 1/a_n$.

If f is a linear function, the coefficient of I_f at frequency ω_n will be $\kappa \cdot v/n \cdot 1/a_n \cdot a_n = \kappa v/n$, where κ is a constant scaling factor introduced by f. Therefore, the spectrum of I_f will be a scaled version of I, i.e., I_f will be contrast reduced step edge function and there will be no ringing artifacts, which is consistent with our conclusion in the linear case.

If f is a non-linear, Farid [35] proved using Taylor series that the coefficients at frequency ω_n for J_f will be scaled non-linearly and non-uniformly, i.e., it will no longer be a scaled version of $v/n \cdot 1/a_n$ and convolving it with K will not cancel out a_n. As a result, I_f will no longer be a step edge function but a signal corrupted by non-uniformly scaled high frequencies. Visually, it will exhibit ringing artifacts. Similar analysis has been carried out in [14].

Effect of Display/Projector Response Function. Eventually, the pre-compensated image is shown on a display or projector for viewing. The emitted irradiance received by viewer will go through a display response function. Since such response functions are always non-linear, the final perceived image by viewer will exhibit stronger ringing artifacts because the high-frequency components of the output signal will be non-uniformly scaled. As a result, it is critical to compensate the display response function before showing the pre-compensated image.

In our experiments, we perform photometric calibration for LCD display and projector using a color checkerboard. We find correspondences between input image intensity and output irradiance and linearize the mapping. Technical details of this calibration process will be described in Section 6. We apply the reverse response function to compensate the non-linearity and re-

duce ringing artifacts in the final output image. Experiments show that by compensating the non-linear projector response curve, the perceived images have higher contrast and less ringing. Please note that this procedure is designed for linear images captured by digital cameras. To combine better viewing experience with minimized ringing, a pre-calibrated non-linear display response function is applied to the original sharp image *prior to* our pre-compensation algorithm. (The response function is based on the pre-calibrated quadratic equations described in Section 6.1.)

3.3 Disambiguating Contrast from Ringing

The existence of ringing poses significant difficulty in measuring contrast. Since ringing appears as oscillating patterns, we cannot directly apply Eqn. 4 as the contrast measure. Specifically, a low contrast image with severe ringing can still produce large RMS contrast (Eqn. 4). In principle, the contrast of a gray-level image should not be modified by ringing, since this artifact does not introduce additional meaningful content. However, the RMS contrast will be artificially boosted due to intensity variance. Alternative contrast definitions such as Weber contrast or Michelson contrast [36] that consider the minimum and maximum luminance are not able to disambiguate actual contrast from ringing. We are not aware of work done on measuring contrast under ringing.

The term "contrast" characterizes a group behavior of pixels. We consider the intensity histograms of the baseline pre-compensated result J_l and the general tone mapped result J_f. Our key observation here is that J_l contains ringing due the Gibbs phenomenon by deconvolution. Further, deconvolution behaves as derivatives of a natural image, and as such, the intensity histogram $H(J_l)$ follows the Laplacian distribution. In Fig. 2(a), we randomly select 5 images from the BSDS500 database [34] and compute their pre-compensated images using a fixed kernel. In Fig. 2(b), we fix the image but apply 6 different kernels to pre-compensated the image. The intensity histograms of the resulting pre-compensated images consistently follow the Laplacian distribution. More examples are included in the supplemental material.

Next, let us consider how a tone mapping function f transforms $H(J_l)$. For the linear function f_m, the offset b shifts the histogram whereas the slope m stretches it. In the non-linear case, we can conduct a first order approximation to f by using the tangent line at the mode of $H(J_l)$ (i.e., the most frequent intensity). This leads to a new contrast factor measure under an arbitrary tone mapping function f: we first compute $H(J_l)$ and
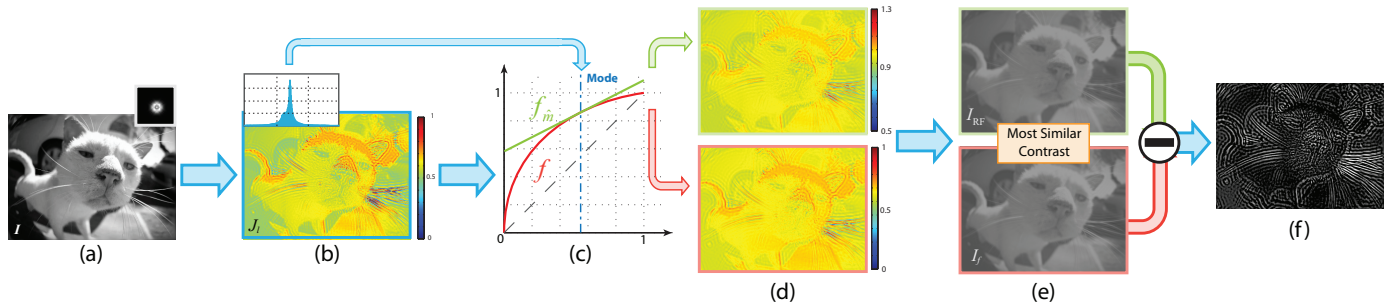
Fig. 3. Measuring contrast and ringing under non-linear tone mapping f. (a) The sharp reference image I and kernel K; (b) The baseline pre-compensated image J_l and its histogram $H(J_l)$; (c) We compute the tangent line $f_{\hat{m}}$ of f at the mode of $H(J_l)$; (d) Linear tone mapping using m produces ringing free result I_{RF} whereas f produces ringing-corrupted result I_f; (e) The contrast of I_f is nearly the same as the contrast of I_{RF}; (f) $|I_{\mathrm{RF}} - I_f|$ approximates the ringing in I_f.

locate mode $\hat{J}_l$; next, we compute the tangent line $f_{\hat{m}}$ on f at point $\hat{J}_l$; finally, we use $f_{\hat{m}}$ to linearly tone map J_l to $J_{f_{\hat{m}}}$.

Since $f_{\hat{m}}$ is linear, $I_{f_{\hat{m}}} = J_{f_{\hat{m}}} \otimes K$ does not induce ringing. We call $I_{f_{\hat{m}}}$ the "equivalent ringing free" image of I_f and denote it as I_{RF}. We then compute the contrast of I_{RF} using Eqn. 4 and treat it as the contrast of I_f. Moreover, computing I_{RF} has another use: we now can quantitatively measure ringing of I_f as $\Gamma = |I_f - I_{\mathrm{RF}}|$. This is consistent with the observation that ringing depends on both the input pre-compensated image J_l (by which we locate the mode of $H(J_l)$) and the tone mapping function f (by which we compute the tangent function at the mode). Fig. 3 shows the complete pipeline for measuring the contrast and ringing under an arbitrary f.

4 TONE MAPPING FUNCTION SELECTION

Our quantitative measures of contrast and ringing enables reliable comparisons between various tone mapping functions and feasible constructions of tone mapping function to achieve specific contrast.

4.1 Contrast-Priority Tone Mapping

We first show how to construct a tone mapping function to achieve a specific contrast. Given a desired contrast factor ζ, we can directly compute the slope m of the corresponding linear mapping function using Eqn. 7 as $m = r \cdot \zeta$. Since ζ is expected to outperform the baseline function f_l and at the same time should not exceed the contrast of the original image, we should restrict ζ as $1/r < \zeta \leq 1$ so that the $m \in (1, r]$.

Our contrast measure analysis shows that, for a tone mapping function f, if we want to maintain contrast m of I_f, at the histogram mode $\hat{J}_l$, f should 1) map $\hat{J}_l$ to $\hat{J}_l$ to preserve the overall image intensity level and 2) should have the tangent slope m at $\hat{J}_l$.

Given these two conditions, we insert an anchor point $P = (\hat{J}_l, \hat{J}_l)$ with tangent m. Recall that the other two anchor points are the endpoints $P^- = (0,0)$ and $P^+ = (1,1)$. Our goal is to construct two Bézier curves, the lower half B^- from P^- to P and the upper half B^+ from P to P^+, to construct f. To do so, we introduce two more anchor points Q^- and Q^+ on the tangent line at P to control the tangent at P^- and P^+. Specifically, we can parameterize Q^- and Q^+ by τ^- and τ^+:

$$
\begin{aligned}
Q^- &= (\hat{J}_l - \tau^- \sin\theta, \hat{J}_l - \tau^- \cos\theta), \\
Q^+ &= (\hat{J}_l + \tau^+ \sin\theta, \hat{J}_l + \tau^+ \cos\theta),
\end{aligned}
\tag{8}
$$

where $\theta = \arctan(1/m)$ and $0 < \tau^- \leq \hat{J}_l / \cos\theta$ and $0 < \tau^+ \leq (1 - \hat{J}_l)/\cos\theta$. As a result, P^-, Q^-, and P form Bézier curve B^- and P, Q^+, and P^+ form Bézier curve B^+ as

$$
\begin{aligned}
B^-(t) &= (1-t)^2 P^- + 2(1-t)t Q^- + t^2 P, \\
B^+(t) &= (1-t)^2 P + 2(1-t)t Q^+ + t^2 P^+, \\
&\text{where} \quad 0 \leq t \leq 1.
\end{aligned}
\tag{9}
$$

By adjusting τ^- and τ^+ and hence Q^- and Q^+, we can control the amount of ringing through the curvature of the curves (Section 3.3) while maintaining the desirable contrast, as shown in Fig 4. We call this set of functions the *adaptive contrast-priority* tone mapping (analogous to shutter/aperture-priority in photography).

Notice that the upper-half Bézier segment B^+ is convex and the lower-half B^- is concave, forming an "S" shape. We therefore denote the special mapping function as s. Fig. 4 shows the results by using different s functions. The reason that the S-shaped curve s achieves higher contrast factor than the baseline mapping l can also also explained using Jensen's inequality: since the upper-half (the high intensity portion) is convex, by Jensen's inequality we have

$$
I_s = B^+(J_l) \otimes K > B^+(J_l \otimes K) > J_l \otimes K = I_l.
\tag{10}
$$

This implies that the brightest pixel in I_s will be brighter than the one in the baseline result I_l. Similarly, since the lower half is concave, the darkest pixel in I_s will be dimmer than the one in I_l. Therefore, the overall dynamic range of final outputs using s will be greater than the one using l.

Next, let us compare s with the classical power mapping function. Recall that the power function, *i.e.*, $g(x) = x^\gamma$, can be either convex when $\gamma > 1$ (denoted as g^+) or concave when $\gamma < 0$ (denoted as g^-) where both types can be used as the tone mapping function. For g^+, similar conclusion of Eqn. 10 holds, *i.e.*, the brightest pixel in I_{g^+} will be brighter than the one in I_l. However, since g^+ is convex everywhere, the dimmest pixel will also be brighter than the baseline result. Therefore, the overall dynamic range is only marginally expanded. Similar arguments apply to g^- which uniformly brings down the intensity for all pixels. Our s function, in contrast, can be viewed as combining the advantage of high intensity potion of g^+ and low intensity portion of g^- and hence outperforms both.
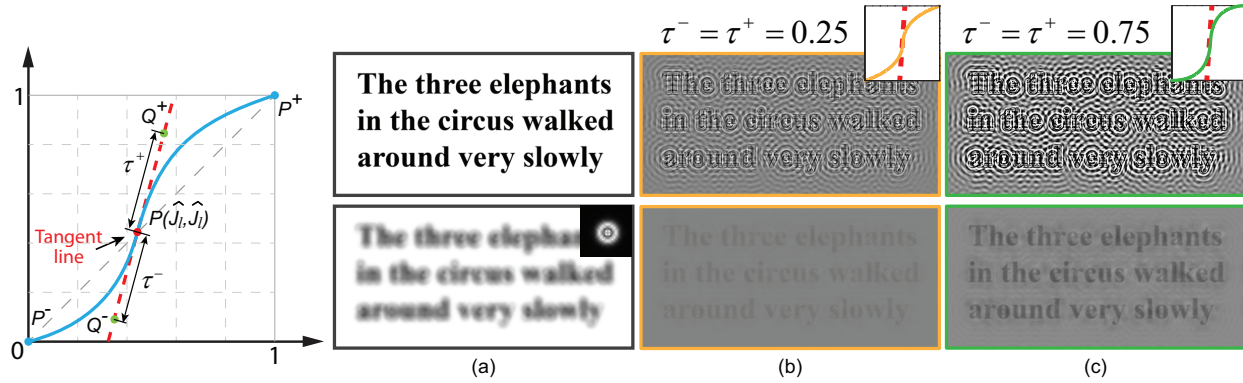
Fig. 4. Left: The construction of an s function. Right: Tone mapping the pre-compensated result using different s functions: (a) The original image and its defocused projection without image pre-compensation; (b) & (c) are tone mapped and final perceived results by applying different s functions.

4.2 Trading Off between Contrast and Ringing

Recall that the linear mapping f_m produces ringing free result I_{RF}. Therefore, we can find the optimal s function that is close to I_{RF}. Specifically, we minimize the following objective function:

$$\mathcal{O}(\tau^-, \tau^+; m) = ||I_{RF}(m) - I_s(\tau^-, \tau^+; m)|| + \alpha \frac{1}{m}. \quad (11)$$

The first term measures the ringing in terms of the different between I_s and its equivalent ringing-free I_{RF}. The second term $1/m$ measures the contrast, *i.e.*, the larger m ($1 < m \leq r$), the higher the contrast. Finally, α is the parameter that trades off between ringing and contrast. A larger α prefers more contrast (larger m) whereas a smaller α prefers ringing-free (the curve will be closer to being linear). In Section 6.2, we conduct a study to choose preferred α for specific types of scenes.

For a given α, we can use the Levenberg-Marquardt (LM) algorithm [37] to minimize the objective function. Specifically, we initialize m to its maximum, *i.e.*, $m = r$ as initial value and find the τ^- and τ^+ that produce the least ringing by minimizing the first term. We then use the resulting τ^- and τ^+ as initial values to optimize m. We apply several iterations to obtain the satisfactory results (the optimization converges within seven iterations in most of our experiments). Fig. 5 shows the optimized results of different α.

5 CONTENT AWARE PRE-COMPENSATION

The human vision system deems some regions in a scene to be more important (i.e., more salient) than others. Based on this observation, we propose to prioritize the contrast preservation in salient regions in order to improve the quality of perceived pre-compensation image. Since visual saliency is determined by image content, we call our algorithm content aware pre-compensation. In this section, we describe our algorithm in details.

Given sharp reference image I, we first detect the salient regions that may attract more attention. Saliency detection [38] is a well studied area in computer vision; it has been used in applications such as object detection and recognition [39], visual tracking [40], and content-based image segmentation [41]. Many computational saliency models have been proposed. A comprehensive survey can be found in [42]. In our work, we adopt the graph-based visual saliency (GBVS) detection algorithm [43], [44] to find salient visual content in the sharp reference image. This algorithm simulates human eye fixation with good fidelity.
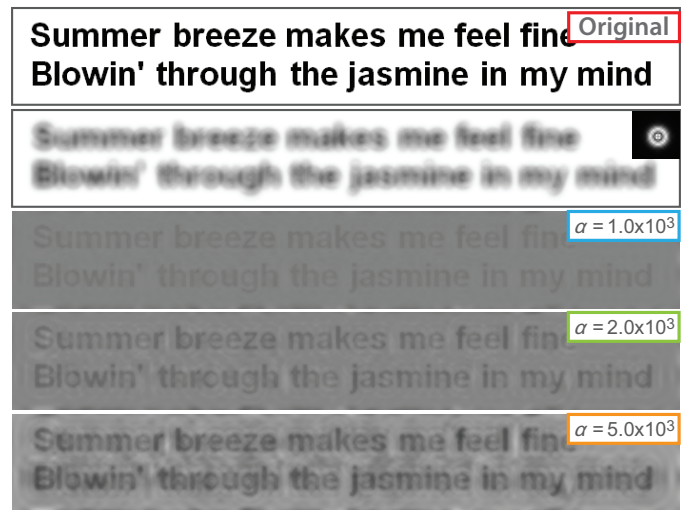

Fig. 5. Balance between contrast and ringing. The top two rows show the reference image and the blurred result if we do not pre-compensate the input. The bottom three rows show the results under different tone mapping functions. Smaller α leads to more contrast loss but incurs minimal ringing. Larger α enhances the contrast but incurs more ringing.

We then use the saliency mask M to separate the reference image I into salient image (foreground) I_M and non-salient (background) image $I_{\bar{M}}$, where $I_M = I * M$ and $I_{\bar{M}} = I * \bar{M}$ ($\bar{M}$ is the inverse mask: $\bar{M} = 1 - M$). We apply a Gaussian filter on the original saliency mask in order to achieve smooth transition from foreground to background; for a 1200×900 image, we use a 51×51 Gaussian filter with $\sigma = 8$. We pre-compensate the salient image I_M and use its contrast loss to guide the optimization of the adaptive contrast-priority tone mapping function in order to preserve the contrast of salient regions at best. In particular, the pre-compensated salient image is computed by applying the inverse blur kernel: $J_M = I_M \otimes K^{-1}$.

Since J_M contains only salient content, we then combine J_M with the background image to obtain an initial estimation of pre-compensated image $\hat{J} = J_M + I_{\hat{M}}$. Note that while the dynamic range of $\hat{J}$ exceeds the limit of $[0, 1]$ due to deconvolution, the range is dominated by the salient image. Comparing the naïve approach that treat the entire image equally, our saliency-based approach eliminates the contrast loss caused by pre-compensating

---

Algorithm 1: Content Aware Image Pre-Compensation

Input : Reference Sharp image I & blur kernel K
Output: Pre-compensated image J
Compute a saliency mask M from $I_{\bar{M}}$;
Compute the inverse mask: $\bar{M} = 1 - M$;
Separate salient image I_M and background image $I_{\bar{M}}$,
where $I_M = I * M$ and $I_{\bar{M}} = I * \bar{S}$;
Pre-compensate salient image $J_M = I_M \otimes K^{-1}$;
Composite an initial pre-compensated image
$\quad \hat{J} = J_M + I_{\bar{M}}$;
Compute the dynamic range of $\hat{J}$: $r = max(\hat{J}) - min(\hat{J})$;
Linear compress $\hat{J}$: $\hat{J}_l = l(\hat{J})$;
Initialize an equivalent ringing-free image $I_{RF}(m_0)$:
$m_0 \leftarrow r$
$I_{RF}(m_0) \leftarrow (m_0\hat{J} + b) \otimes K$;
Iteratively optimize the adaptive contrast-priority tone
    mapping function s until convergence or reaching the
    maximum iteration.
while $k < iter_{max}$ **and** $\mathcal{O}(\tau^-, \tau^+; m) < \epsilon$ **do**
$\quad$ Fix m_k, solve
$\quad\quad \min_{\tau_{k+1}^-, \tau_{k+1}^+} ||I_{RF}(m_k) - I_s(\tau_{k+1}^-, \tau_{k+1}^+; m_k)||$;
$\quad$ Fix $\tau_{k+1}^-, \tau_{k+1}^+$, solve $\min_{m_{k+1}} ||I_{RF}(m_{k+1}) -$
$\quad\quad I_s(\tau_{k+1}^-, \tau_{k+1}^+; m_{k+1})|| + \alpha\frac{1}{m_{k+1}}$;
$\quad$ $k = k + 1$;
end
Compute and output the final pre-compensated image
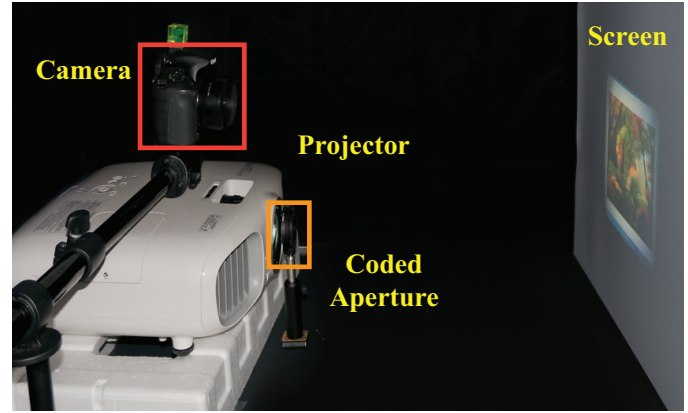$\quad J = s(\hat{J}_l)$

Fig. 6. Experimental setup on projector defocus compensation.

6 EXPERIMENTS

In this section, we validate our content aware pre-compensation algorithm on two applications: projector defocus compensation and visual acuity improvement.

6.1 Projection Defocus Compensation

A projector acts as a camera with an ultra-wide aperture and therefore can only focus at a fixed depth. All projectors suffer from certain blurriness due to imperfect optics or non-planar projection surface. Our algorithm is the first that is able to compensate such blurriness by actively balancing the image contrast and ringing artifacts. In addition, our algorithm prioritizes the contrast of salient visual content.

To validate our approach, we use an Epson Powerlite 3LCD projector to display images on a projection screen; we adjust the projector to be slightly out of focus. We mount a coded aperture (as shown in Fig. 7) for generating invertible PSFs. To estimate the PSFs or blur kernels for image pre-compensation, we project a 36×64 dot array and capture its image. To suppress sensor noise, we capture ten images and take the average. The defocus patterns of the dots are used as blur kernels. To account for chromatic aberration, we consider the PSFs for each color channel separately. On the acquisition side, we use a Canon 60D camera to capture the projected images to simulate the perceived image by a human viewer. We focus the camera on the projection screen and assume defocus is solely caused by the projector. Our experimental setup is shown in Fig. 6.

Projector Response Function Calibration. As discussed in Section 3.2, the non-linearity of projector response function causes ringing artifacts. In order to compensate for the response function, we calibrate the projector response function and apply the inverse function on the displaying image for compensation. Specifically, we project color checkers to establish correspondences between input intensity and output irradiance. In order to eliminate the effect of gamma correction (power function with γ as the exponent), we set $\gamma = 1$ in the projector settings.

Since the projected color field is non-uniform, we calibrate the response function based on local windows. Specifically, we project each color in the color checkerboard one by one in full resolution. We segment the projected image into small non-overlapping windows of 100×100 (in pixels) and estimate the response function per window. For each window, we assume the color is uniform and average the intensities within

the background image and hence better preserve the contrast of salient image content.

We first use the baseline mapping function l to linearly compress the range of $\hat{J}$ to $[0, 1]$. The linearly compressed pre-compensated image is computed as $\hat{J}_l = (\hat{J} - min(\hat{J}))/(max(\hat{J}) - min(\hat{J}))$, and it suffers from severe contrast loss. Next, our goal is to find the optimal contrast-priority tone mapping function in order to enhance the contrast. As described in Section 4.1, our contrast-priority tone mapping function or the S-shaped curve is able to achieve a specific contrast. Therefore, we use best possible contrast of the pre-compensated image to initialize an equivalent ringing-free image I_{RF}. In particular, the initial slope of the corresponding linear mapping function is computed as $m_0 = r \cdot \zeta$, where $r = max(\hat{J}) - min(\hat{J})$ is the dynamic range of $\hat{J}$ and we use the maximum contrast factor ($\zeta = 1$).

Then we iteratively update the two sets of parameters in the contrast-priority tone mapping function (τ^-, τ^+) and m to balance between contrast and ringing. The optimization processed is described in Section 4.2 . As a result, we obtain an optimized contrast-priority tone mapping function s based on the contrast of the pre-compensated salient image.

Finally, we apply the optimized s function onto $\hat{J}_l$ to compute the pre-compensated image that best preserves the contrast of salient image content $J = s(\hat{J}_l)$. The complete process of our content aware pre-compensation is summarized in Algorithm 1.
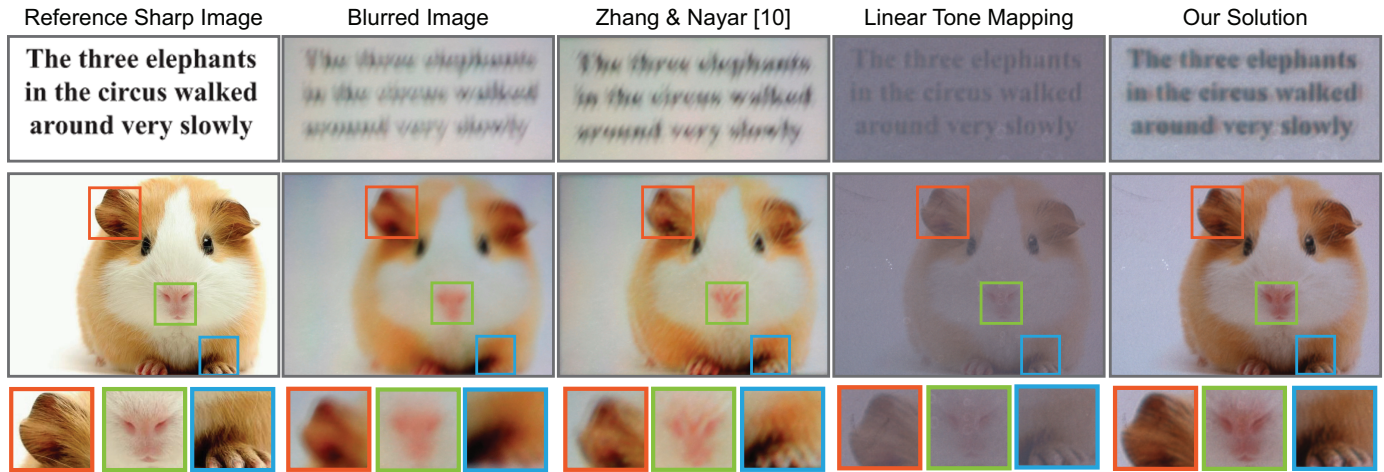
Fig. 7. Projector defocus compensation results. From left to right: reference sharp images; blurred images (without pre-compensation) captured by a camera; pre-compensation results by Zhang and Nayar's algorithm [10], which preserves the contrast but exhibits strong ringing; pre-compensation results by linear tone mapping, which avoids ringing but loses contrast; our pre-compensation results enhance the contrast with only slight ringing.

the window to reduce noise. Our non-linear response function per window consists of three per-channel quadratic equations $\{R_o, G_o, B_o\} = \mathcal{F}_{\{R_o,G_o,B_o\}}(R_i, G_i, B_i)$; for the red channel, it is

$$\begin{aligned} \mathcal{F}_{R_o}(R_i, G_i, B_i) = &\, a_1 R_i^2 + a_2 G_i^2 + a_3 B_i^2 + a_4 R_i B_i \\ &+ a_5 R_i G_i + a_6 B_i G_i + a_7 R_i + a_8 G_i + a_9 B_i + a_{10}, \end{aligned} \quad (12)$$

where R_o is the observed red channel intensity, R_i, G_i, B_i are the corresponding ground truth, and $\{a_1, ..., a_{10}\}$ are the quadratic equation coefficients. $\mathcal{F}_{B_o}$ and $\mathcal{F}_{G_o}$ are similarly defined with different coefficients. To determine these quadratic equations, we estimate their coefficients by solving a large over-determined linear system. Specifically, for each non-linear response, we need to solve 30 coefficients (i.e., 10 for each per-channel quadratic equation) and 72 equations can be constructed by projecting 24 colors in the standard color checkerboard.

Although the projector has a resolution of 1920×1080, we use the center area of 1200×900 to avoid vignetting artifacts at the image periphery caused by our coded aperture. As a result, we obtain 108 non-linear responses (one for each window) and we apply the inverse response functions on the pre-compensated image to reduce the ringing artifacts caused by the non-linear functions.

Evaluation. We compare the results of our proposed content-aware image pre-compensation algorithm with those of competing state-of-the-art techniques. Given a sharp reference I, we first apply the saliency detection algorithm described in [43], [44] to separate salient image content and background. Then, we apply Wiener filter on the salient image and combine with the background image to obtain an initial pre-compensated image J, where the dynamic range of J exceeds the display limit of $[0, 1]$. We then linearly compress J to the range of $[0, 1]$. To preserve the contrast of salient content, we use the contrast loss of the pre-compensated salient image to initialize an equivalent ringing-free image and apply our optimization framework to find the optimal contrast-priority tone mapping curve. In our experiments, we set $\alpha = 1 \times 10^3$. We run our experiments on a laptop computer with Intel Core i7 GPU and 8GB memory. The total running time is around 0.7s (for images with size 1200×900) using Matlab.

Fig. 7 shows results for two representative images. Directly using the linearly compressed pre-compensation produces images with significant reduction in contrast. Results using steepest descent [10] have enhanced contrast, but at the cost of excessive blur. Results produced by our technique appear much sharper with less ringing. This is because our algorithm can handle large blur kernels while [10] only works well on small ones.

In our approach, we can use a larger α to reduce ringing at the cost of losing contrast or a smaller α to enhance contrast at the cost incurring more ringing. In text image result, the texts are hardly discernible in the blurred image, while our approach is able to restore the text with moderate contrast. More results on the natural images are shown in Fig. 13. Here, we can see that our algorithm significantly enhances the image contrast compared to the linear tone mapped results while minimizing ringing. We also compare our result with simple gamma correction (Fig 8). The gamma correction function is applied on the linear compressed pre-compensation image. As can be seen, correction is not effective in enhancing contrast. This is the because it brings out either bright or dark details while the histogram of pre-compensated image is centered around the mean intensity value. Gamma correction is not effective in stretching the dynamic range.

In Fig. 14, we demonstrate the effectiveness of the projector response function correction. We show the pre-compensation results with and without response function correction. As shown in the results, the pre-compensation results with projector response function correction has less ringing and higher contrast. As shown in the close-up views, text and image details appear sharper.

To quantitatively evaluate the results, we use CIE76 ΔE metric to measure the color difference between the perceived pre-compensation image (captured by an in-focus camera) and the reference sharp image. We first transform the color in RGB color into CIELAB space. Given two coordinate in CIELAB space, (L_1, a_1, b_1) and (L_2, a_2, b_2), the ΔE metric is computed as the Euclidean distance between the coordinates:

$$\Delta E = \sqrt{(L_2 - L_1)^2 + (a_2 - a_1)^2 + (b_2 - b_1)^2}. \quad (13)$$

Therefore, the lower the value, the closer the colors of the two images appear. The pre-compensation results with our projector response correction have lower ΔE.
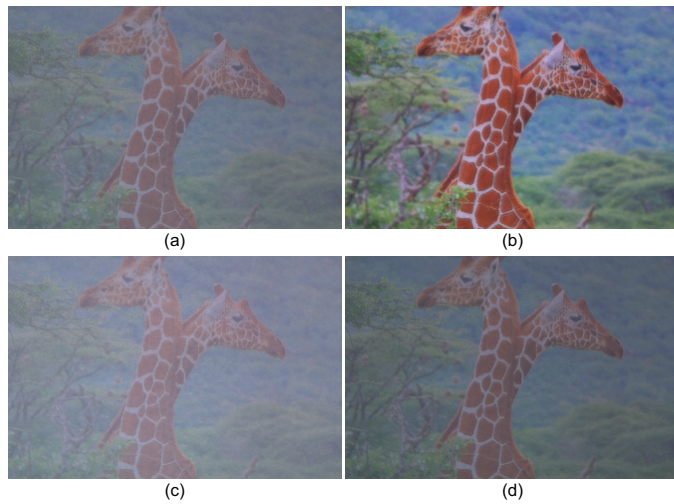
Fig. 8. Comparison with simple gamma correction. (a) Linear tone mapping result; (b) our pre-compensation result; (c) gamma correction result with $\gamma = 1/2.2$; (d) gamma correction result with $\gamma = 1.8$.

We also compare results of our approach with those of our previous algorithm proposed in [17] (Fig. 15). In our previous algorithm, visual saliency is not considered, and the whole image is pre-compensated in one pass. Qualitatively, our results have higher contrast and less ringing, especially on the sharp edges (such as the wings of the parrot and dragonfly). Although our algorithm allow more blurriness in the background, the effect is not noticeable since the backgrounds are already out-of-focus in the reference image. Quantitatively, we compare the results by ΔE (color difference between the simulated perceived image and the original sharp image) and the dynamic range span r ($r = max(I) - min(I)$) of the pre-compensated image. Notice that according to Eqn. 3, the smaller r is, the less contrast loss the final perceived image would suffer. Results produced by our solution have smaller values of both ΔE and r, which means that our simulated perceived images are closer to the sharp reference image and have higher contrast.

We further perform experiments to evaluate the robustness of our algorithm to noise in the blur kernel. Specifically, we add different amounts of synthetic Gaussian noise (1%, 5%, and 10% of the dynamic range [0,255]) to the ground truth PSF and use the noisy PSFs as input to our algorithm for deconvolution. We use images in the BSDS500 dataset [34] as the input sharp reference images and use the PSFs with various noise levels for pre-compensation. The structural similarity (SSIM) index [45] is used to measure quality of the pre-compensation images with the original sharp images as reference. The SSIM values averaged over the entire dataset is shown in Table 2. Visual results for three representative images are shown in Fig. 9. As the PSF noise is increased, SSIM decreases, with the pre-compsation images having more ringing artifacts. However, even with 10% noise added, the visual quality of the pre-compensation image is still reasonable.

6.2 Improving Visual Acuity

There is an emerging interest on developing tailored displays for improving visual acuity, *e.g.*, to allow a person with myopia to read without wearing corrective lenses. Recall that both myopia and hyperopia can be viewed as special defocus blurs. We show

TABLE 2
Effect of PSF noise on SSIM quality metric. SSIM is averaged over 500 images taken from the BSDS500 dataset [34].

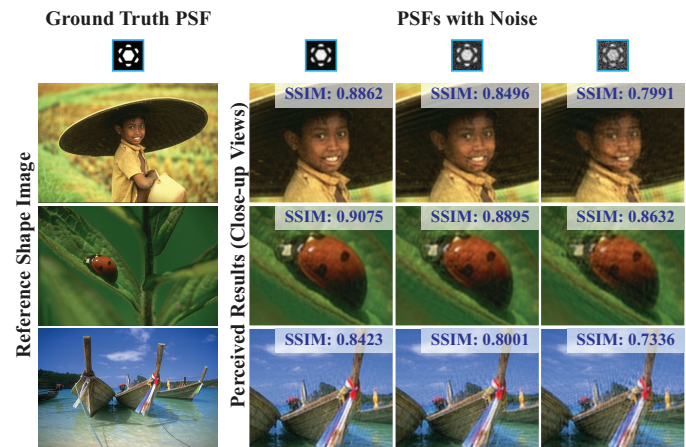| PSF Noise	1%	5%	10%
SSIM	0.8978	0.8394	0.7560

Fig. 9. Effect of PSF noise. Left: original sharp images and the ground truth PSF. Right: Pre-compensation images (with close-ups) and their corresponding PSFs with noise (which increases from left to right, namely, 1%, 5%, and 10%). Notice that while the quality degrades with noise, the visual quality is still reasonable despite the noticeable ringing.

that contrast can be significantly enhanced by maneuvering the tone mapping process and our technique is complementary to the computational display approaches. In this section, we demonstrate the effectiveness of our pre-compensation algorithm in improving visual acuity.

We emulate the PSFs of myopia/hyperopia using Zernike polynomials [46] which are widely adopted in ophthalmology. The kernel in its radial form is defined as

$$R_n^m(\rho) = \sum_{i=0}^{(n-m)/2} \frac{(-1)^i (n-i)!}{i!(\frac{1}{2}(n+m)-i)!(\frac{1}{2}(n-m)-i)!} \rho^{n-2i},$$
(14)

where $0 \leq m \leq n$ and $n - m$ is even. In our experiments, we only consider up to the second order ($n \leq 2$) terms which can sufficiently model defocus and astigmia. Fig 12(b) shows several examples of our PSFs that correspond to different levels of vision degradation.

We emulate the effect of myopia by convolving sharp text images with the PSFs and display the results on a regular LCD display Viewsonic VA2448 with contrast ratio 1000:1. We then use our algorithm to find the pre-compensated text images that, after

Fig. 10. Emulation of myopia by displaying blurred text. Left to right: blurred text using the myopia kernel, result using pre-compensated image under linear tone mapping, result using our approach.
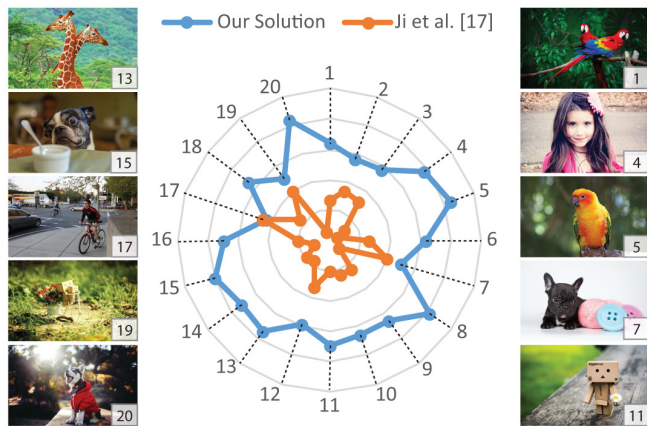
Fig. 11. A user study for evaluating our system. We show ten samples out of our twenty test images. In our circle plot, each radius corresponds to a test image. The blue point on each radius refers to the number of users who pick the pre-compensation result of our approach and the orange point refers to the number of users who pick the result of Ji et al. [17]. We can see that for most images, more users prefer the results of our approach over those of Ji et al. [17].

being blurred by the myopia PSFs, will appear readable to the user. Compared with the projector defocus case where the reference image I is generally a natural image with rich color and contrast, the reference images for this application are grayscale or even black/white to represent typical texts (*e.g.*, displayed on Kindle). Compared with linear tone mapping, our technique significantly enhances the contrast as shown in Fig. 10.

User Studies. Finally, we perform a user study to test the effectiveness of our approach. We have recruited 45 subjects (34 male, 11 female), with an average age of 23. Subjects perform the test with corrected vision and the pre-compensation results are shown on a LCD display after being blurred by their myopia PSFs. We select 10 different myopia PSFs and 20 different images. The ten images used are shown in Fig. 11. For each user, we perform two sets of experiments. In the first experiment, we ask the users to compare the pre-compensation results of our approach and Ji et al. [17], and pick one that is more visually preferable. The goal of this experiment is to demonstrate the effectiveness of using saliency to enhance contrast. The user preference results are shown in Fig. 11; for most images, more users prefer the results of our new saliency-based pre-compensation algorithm. One exception is Test Image 17 (this image is shown in Fig. 11). For this image, slightly more users pick the result of Ji et al. [17]. This is probably due the saliency detection result is not desirable (saliency masks are shown in our supplemental material).

In the second experiment, we study the effect of our contrast/ringing control factor α (see Eqn. 11). α is the parameter that trades between ringing and contrast. A larger α prefers higher contrast whereas a smaller α tolerates more ringing-free. We have developed an interface to allow the user to dynamically change α and view the pre-compensation results. The users are asked to adjust α under two scenarios: 1) given a fixed blur kernel (PSF), adjust α for different text images; 2) give a fixed test image, adjust α for different PSFs. For every PSF and test image pair, each user tunes to his/her favorite α that produces the most agreeable result. Our results are shown in Fig. 12 where (a) and (b) are the variations of α with respect to the text images and PSFs respectively. This study indicates that the preferable α is relatively
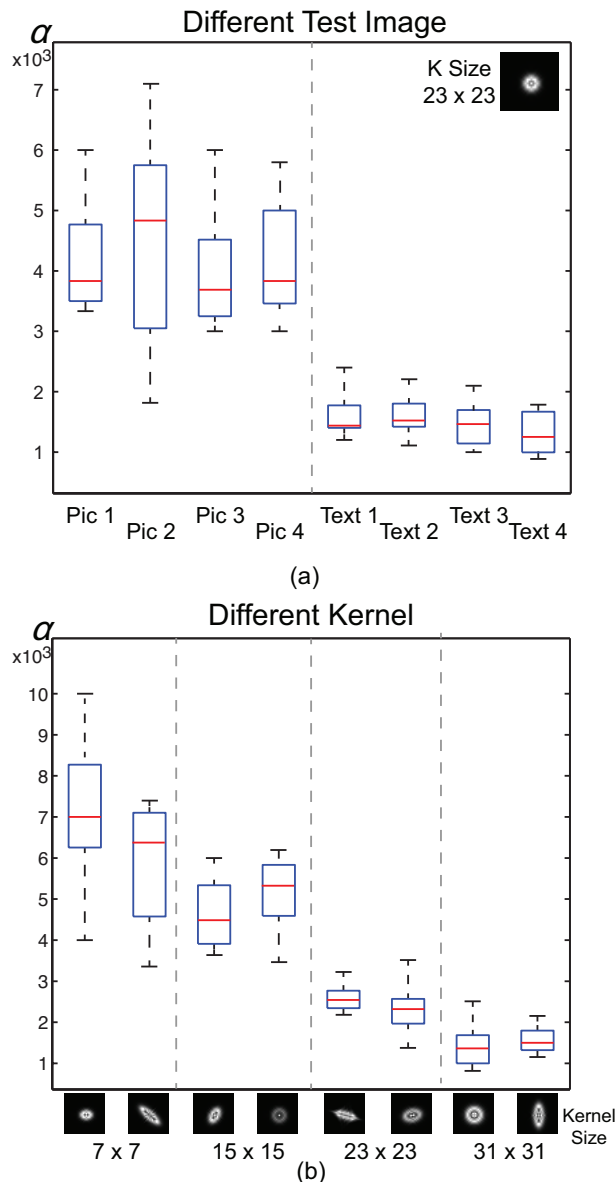

(a)

(b)

Fig. 12. User preference on α. (a) For a fixed kernel, we plot the range of preferred α across users on different test images. (b) For a fixed test image, we plot the range of preferred α across the users on different kernels. The red bar corresponds to the mean α.

consistent across users, although it changes with respect to the image content and the PSF.

7 CONCLUSIONS AND FUTURE WORK

We present a new tone mapping approach for image pre-compensation that effectively trades off between contrast and ringing. We also provide in-depth analysis on the causes of dynamic range burst and ringing. Furthermore, we develop a technique to measure contrast and ringing on images in image pre-compensation. Based on our analysis, we design a contrast-preserving tone mapping function. To enhance contrast, we use the contrast loss in salient regions to guide the search of optimal contrast-preserving tone mapping function. We demonstrate our approach on two important applications: projector defocus compensation and corrective lens free visual enhancement. Compared with the state-of-the-art, our approach not only greatly improves

the contrast but also provides an effective interface to trade between contrast and ringing.

Although our user study in visual acuity enhancement illustrates the effectiveness of our solution, more can be done. More specifically, the next step would be to measure the actual myopia/hyperopia PSFs of each individual user, *e.g.*, by using the tailored display [31] and use the ground truth PSFs to estimate the tone mapping function. In addition, our Bezier curve model is used to replicate the contrast at the most frequent intensity only. If the histogram of the pre-compensated image has multiple peaks, we can potentially insert multiple anchor points and construct a more complex tone-mapping function. Finally, the problem of contrast preservation can be studied from the perspective of gradients [47]. Our tone mapping function is global and in the future, we plan to explore integrating our contrast model with gradient histogram and gradient domain fusion for handling local contrast enhancement.

ACKNOWLEDGMENT

REFERENCES

[1] Y. Yitzhaky, I. Mor, A. Lantzman, and N. S. Kopeika, "A direct method for restoration of motion blurred images," *Journal of the Optical Society of America A: Optics, Image Science, and Vision*, vol. 15, pp. 1512–1519, 1998.

[2] A. Levin, "Blind motion deblurring using image statistics," *Proceedings of Neural Information Processing Systems (NIPS)*, 2006.

[3] R. Liu, Z. Li, and J. Jia, "Image partial blur detection and classification," *Proceedings of IEEE Conference on Computer Vision and Pattern Recognition (CVPR)*, 2008.

[4] D. Krishnan and R. Fergus, "Fast image deconvolution using hyper-laplacian priors," *Proceedings of Neural Information Processing Systems (NIPS)*, vol. 22, pp. 1–9, 2009.

[5] A. Levin, R. Fergus, F. Durand, and W. T. Freeman, "Image and depth from a conventional camera with a coded aperture," *ACM Transactions on Graphics (also Proc. of ACM SIGGRAPH)*, Jul 2007.

[6] N. Joshi, R. Szeliski, and D. Kriegman, "PSF estimation using sharp edge prediction," in *Proceedings of IEEE Conference on Computer Vision and Pattern Recognition (CVPR)*, 2008.

[7] N. Joshi, C. L. Zitnick, R. Szeliski, and D. J. Kriegman, "Image deblurring and denoising using color priors," in *Proceedings of IEEE Conference on Computer Vision and Pattern Recognition (CVPR)*, 2009.

[8] S. Cho and S. Lee, "Fast motion deblurring," in *ACM SIGGRAPH Asia*, 2009.

[9] X. Chen, F. Li, J. Yang, and J. Yu, "A theoretical analysis of camera response functions in image deblurring," in *Proceedings of European Conference on Computer Vision (ECCV)*, 2012.

[10] L. Zhang and S. K. Nayar, "Projection Defocus Analysis for Scene Capture and Image Display," *ACM Transactions on Graphics (also Proc. of ACM SIGGRAPH)*, Jul 2006.

[11] M. S. Brown, P. Song, and T.-J. Cham, "Image pre-conditioning for out-of-focus projector blur," in *Proceedings of IEEE Conference on Computer Vision and Pattern Recognition (CVPR)*, 2006.

[12] Y. Oyamada and H. Saito, "Focal pre-correction of projected image for deblurring screen image," in *Proceedings of IEEE Conference on Computer Vision and Pattern Recognition (CVPR)*, 2007.

[13] S. Kim, Y.-W. Tai, S. J. Kim, M. Brown, and Y. Matsushita, "Nonlinear camera response functions and image deblurring," in *Proceedings of IEEE Conference on Computer Vision and Pattern Recognition (CVPR)*, 2012.

[14] Y.-W. Tai, X. Chen, S. Kim, S. J. Kim, F. Li, J. Yang, J. Yu, Y. Matsushita, and M. S. Brown, "Nonlinear camera response functions and image deblurring: Theoretical analysis and practice," *IEEE Transactions on Pattern Analysis and Machine Intelligence*, vol. 35, no. 10, pp. 2498–2512, 2013.

[15] M. Alonso, Jr., A. Barreto, and J. G. Cremades, "Image pre-compensation to facilitate computer access for users with refractive errors," in *Proceedings of ACM SIGACCESS conference on Computers and accessibility*, 2004.

[16] F.-C. Huang, D. Lanman, B. A. Barsky, and R. Raskar, "Correcting for optical aberrations using multilayer displays," *ACM Transactions on Graphics (also Proc. of ACM SIGGRAPH Asia)*, vol. 31, Nov. 2012.

[17] Y. Ji, J. Ye, S. B. Kang, and J. Yu, "Image pre-compensation: Balancing contrast and ringing," in *Proceedings of IEEE Conference on Computer Vision and Pattern Recognition (CVPR)*, 2014, pp. 3350–3357.

[18] Q. Shan, J. Jia, and A. Agarwala, "High-quality motion deblurring from a single image," *ACM Transactions on Graphics*, vol. 27, no. 3, 2008.

[19] S. Cho, J. Wang, and S. Lee, "Handling outliers in non-blind image deconvolution," in *Proceedings of International Conference on Computer Vision (ICCV)*, Nov 2011, pp. 495–502.

[20] T. Kenig, Z. Kam, and A. Feuer, "Blind image deconvolution using machine learning for three-dimensional microscopy," *IEEE Transactions on Pattern Analysis and Machine Intelligence (TPAMI)*, vol. 32, no. 12, pp. 2191–2204, Dec 2010.

[21] W. H. Richardson, "Bayesian-based iterative method of image restoration∗," *J. Opt. Soc. Am.*, vol. 62, no. 1, pp. 55–59, Jan 1972.

[22] L. Xu, J. S. J. Ren, C. Liu, and J. Jia, "Deep convolutional neural network for image deconvolution," in *Advances in Neural Information Processing Systems (NIPS)*, ser. NIPS'14, 2014, pp. 1790–1798.

[23] M. Alonso and A. B. Barreto, "Pre-compensation for high-order aberrations of the human eye using on-screen image deconvolution," in *Proceedings of the 25th Annual International Conference of the IEEE Engineering in Medicine and Biology Society (IEEE Cat. No.03CH37439)*, vol. 1, Sept 2003, pp. 556–559 Vol.1.

[24] M. A. Jr., A. Barreto, and M. Adjouadi, "Digital image inverse filtering for improving visual acuity for computer users with visual aberrations," *Inverse Problems in Science and Engineering*, vol. 16, no. 8, pp. 957–966, 2008.

[25] C. Montalto, I. Garcia-Dorado, D. Aliaga, M. M. Oliveira, and F. Meng, "A total variation approach for customizing imagery to improve visual acuity," *ACM Trans. Graph.*, vol. 34, no. 3, pp. 28:1–28:16, May 2015.

[26] M. G. K. Fujii and S. Nayar, "A projector-camera system with real-time photometric adaptation for dynamic environments," in *Proceedings of IEEE Conference on Computer Vision and Pattern Recognition (CVPR)*, 2005, pp. 814–821.

[27] M. G. S.K. Nayar, H. Peri and P. Belhumeur, "A projection system with radiometric compensation for screen imperfections," in *Proceedings of ICCV Workshop on Projector-Camera Systems (PROCAMS)*, 2003.

[28] S. N. M.D. Grossberg, H. Peri and P. Belhumeur, "Making one object look like another: Controlling appearance using a projector-camera system," in *Proceedings of IEEE Conference on Computer Vision and Pattern Recognition (CVPR)*, 2004, pp. 425–459.

[29] M. Grosse, G. Wetzstein, A. Grundhoefer, and O. Bimber, "Coded aperture projection," *ACM Transactions on Graphics*, vol. 29, no. 3, pp. 1–12, 2010.

[30] B. Masia, G. Wetzstein, P. Didyk, and D. Gutierrez, "A survey on computational displays: Pushing the boundaries of optics, computation, and perception," *Computers & Graphics*, vol. 37, no. 8, pp. 1012 – 1038, 2013.

[31] V. F. Pamplona, M. M. Oliveira, D. G. Aliaga, and R. Raskar, "Tailored displays to compensate for visual aberrations," *ACM Transactions on Graphics*, vol. 31, no. 4, pp. 81:1–81:12, Jul. 2012.

[32] F.-C. Huang and B. A. Barsky, "A frame work for aberration compensated displays," University of California, Berkley, Tech. Rep. UCB/EECS-2011-162, Dec 2011.

[33] J. G. Proakis and D. G. Manolakis, *Digital signal processing*, 4th ed. NJ, USA: Pearson Prentice Hall, 2006.

[34] D. Martin, C. Fowlkes, D. Tal, and J. Malik, "A database of human segmented natural images and its application to evaluating segmentation algorithms and measuring ecological statistics," in *Proceedings of International Conference on Computer Vision (ICCV)*, vol. 2, July 2001, pp. 416–423.

[35] H. Farid, "Blind inverse gamma correction," *IEEE Transactions on Image Processing*, vol. 10, no. 10, pp. 1428–1433, Oct 2001.

[36] E. Peli, "Contrast in complex images," *Journal of the Optical Society of America A*, vol. 7, no. 10, pp. 2032–2040, Oct 1990.

[37] J. Moré, "The Levenberg-Marquardt algorithm: Implementation and theory," in *Numerical Analysis*, ser. Lecture Notes in Mathematics. Springer Berlin / Heidelberg, 1978, ch. 10, pp. 105–116.

[38] L. Itti, C. Koch, and E. Niebur, "A model of saliency-based visual attention for rapid scene analysis," *IEEE Transactions on Pattern Analysis and Machine Intelligence (TPAMI)*, vol. 20, no. 11, pp. 1254–1259, 1998.

[39] U. Rutishauser, D. Walther, C. Koch, and P. Perona, "Is bottom-up attention useful for object recognition?" in *Proceedings of IEEE Conference on Computer Vision and Pattern Recognition (CVPR)*, 2004.
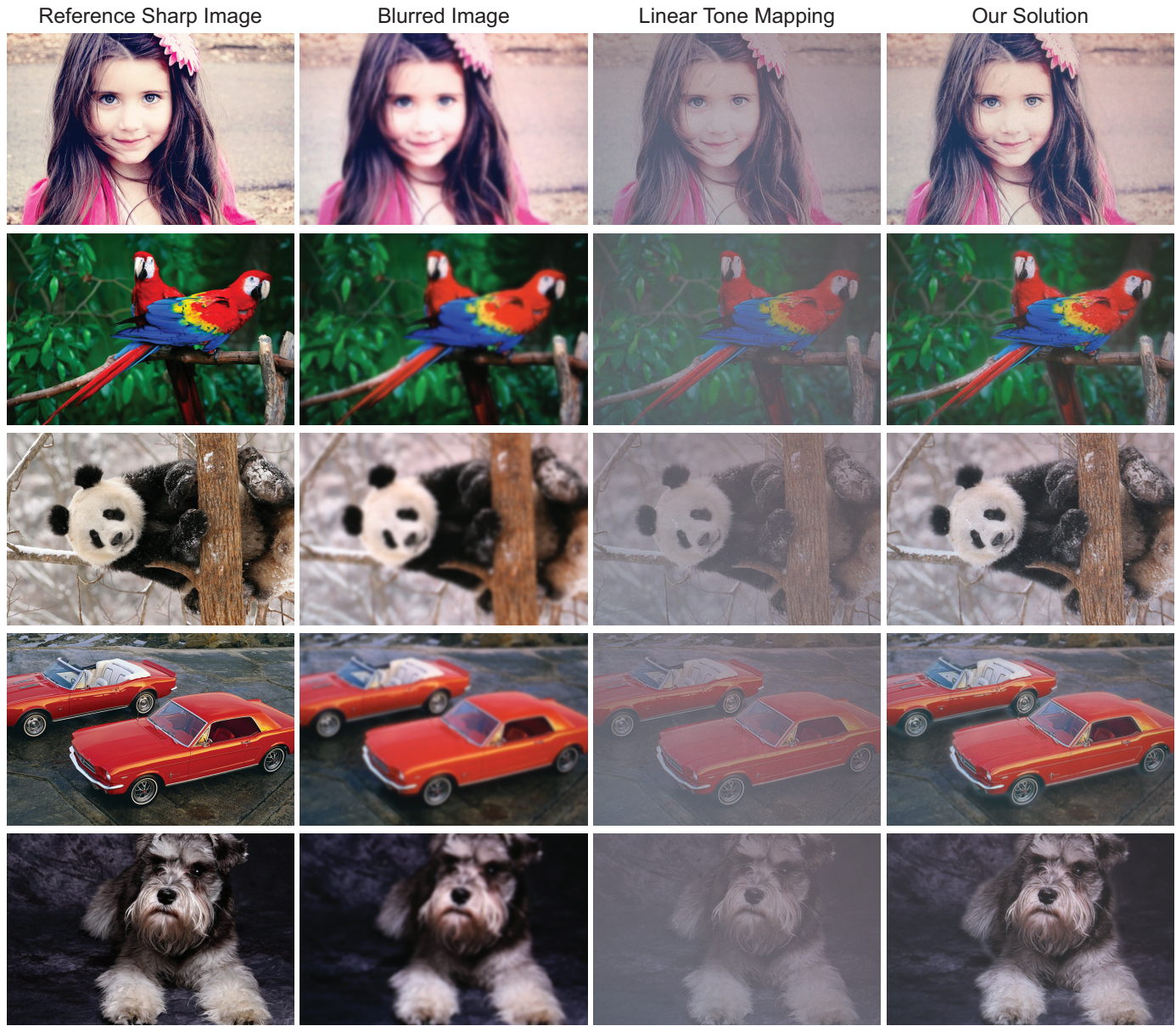
Fig. 13. Additional Projector defocus compensation results. From left to right: reference sharp images; blurred images (without pre-compensation) captured by a focused camera; pre-compensation results by linear tone mapping; our pre-compensation results.

[40] J. Li, M. D. Levine, X. An, X. Xu, and H. He, "Visual saliency based on scale-space analysis in the frequency domain," *IEEE Transactions on Pattern Analysis and Machine Intelligence*, vol. 35, no. 4, pp. 996–1010, April 2013.

[41] M. Donoser, M. Urschler, M. Hirzer, and H. Bischof, "Saliency driven total variation segmentation," in *International Conference on Computer Vision (ICCV)*, Sept 2009, pp. 817–824.

[42] A. Borji, M. M. Cheng, H. Jiang, and J. Li, "Salient object detection: A benchmark," *IEEE Transactions on Image Processing*, vol. 24, no. 12, pp. 5706–5722, 2015.

[43] J. Harel, C. Koch, and P. Perona, "Graph-based visual saliency," in *Advances in Neural Information Processing Systems (NIPS)*, 2007, pp. 545–552.

[44] J. HarelC. A saliency implementation in matlab. [Online]. Available: http://www.klab.caltech.edu/ harel/share/gbvs.php

[45] Z. Wang, A. C. Bovik, H. R. Sheikh, and E. P. Simoncelli, "Image quality assessment: from error visibility to structural similarity," *IEEE Transactions on Image Processing*, vol. 13, no. 4, pp. 600–612, April 2004.

[46] J. Y. Wang and D. E. Silva, "Wave-front interpretation with zernike polynomials," *Applied Optics*, vol. 19, no. 9, pp. 1510–1518, May 1980.

[47] R. Fattal, D. Lischinski, and M. Werman, "Gradient domain high dynamic range compression," *ACM Transactions on Graphics (also Proc. of ACM SIGGRAPH)*, vol. 21, no. 3, pp. 249–256, Jul. 2002.
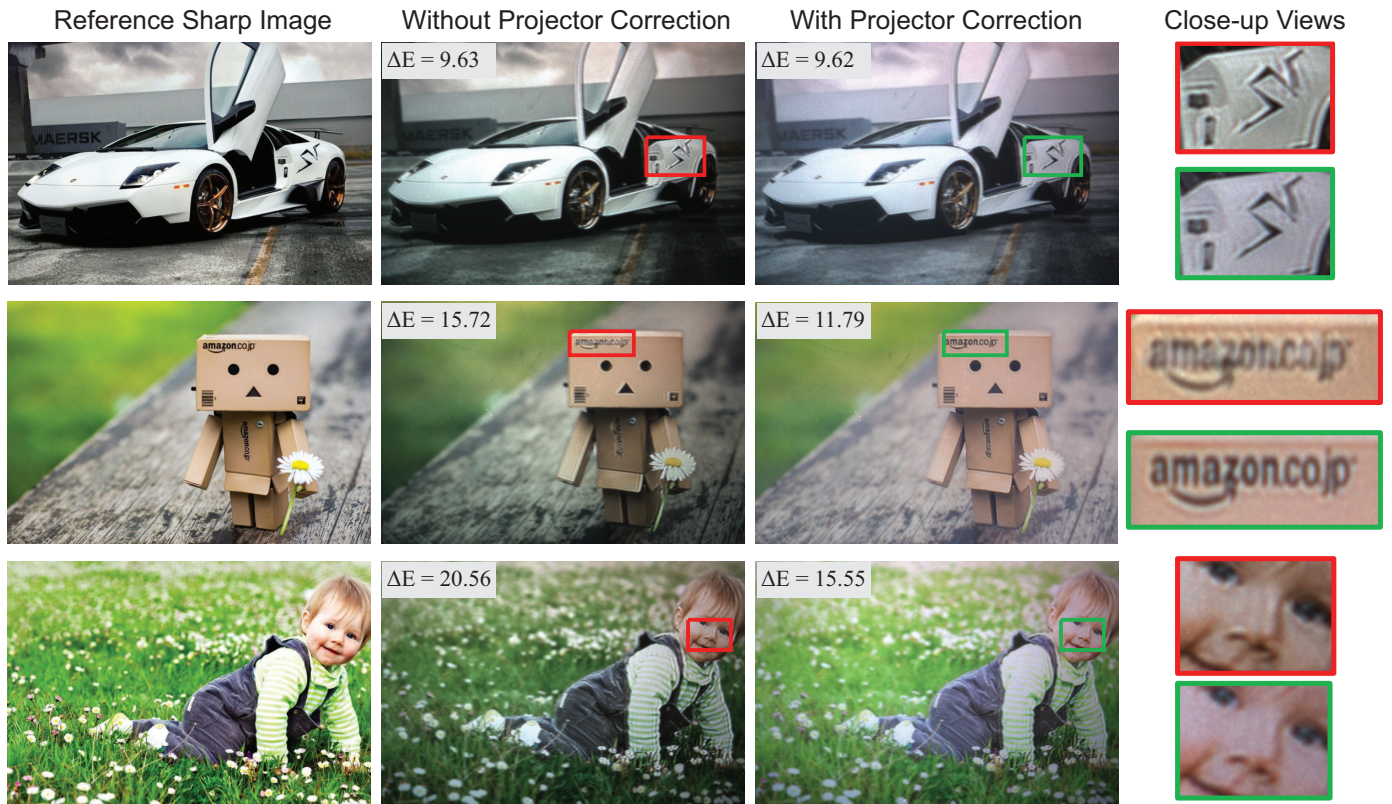
Fig. 14. We compare the pre-compensation results with and without projector response function correction. From left to right: reference sharp images; pre-compensation results with projector correction; pre-compensation results without projector correction; close-up views in the pre-compensated images. The CIE76 ΔE metric is used to measure the color difference; the smaller ΔE is, the better.


Fig. 15. We compare our pre-compensation results with Ji *et al.* [17]. From left to right: reference sharp images; pre-compensation results by Ji *et al.* [17]; pre-compensation results by our approach; close-up views in the pre-compensated images. The CIE76 ΔE metric is used to measure the color difference; the smaller ΔE is, the better. r represents contrast loss; the smaller r is, the better.

Jinwei Ye received her PhD degree from University of Delaware in 2014. She received her B.Eng. in Electrical Engineering from Huazhong University of Science and Technology. After her PH.D., she worked with the US Army Research Laboratory (ARL) and Canon U.S.A., Inc. Currently, she is an assistant professor at the Division of Computer Science and Engineering at Louisiana State University. Her research interests lie in the fields of computational photography and computer vision.

Yu Ji received his PhD degree in computer science from the University of Delaware in 2014. He received his M.Sc. in digital media from Nanyang Technological University in 2011 and Bachelor degree in Electrical Engineering from Huazhong University of Science and Technology in 2009. He is now a principal scientist at Plex VR. His research interests include computational photography, computer vision, and computer graphics.
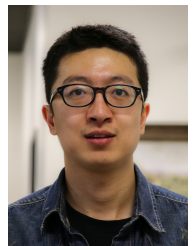
Mingyuan Zhou received his M.E. degree in Computer Engineering from Stevens Institute of Technology in 2014, and B.E. degree in Intelligence Science and Technology from Beijing Information Science and Technology University, China, in 2011. He is now a Ph.D. student at the Department of Computer and Information Sciences, University of Delaware. His research interests include image processing, computer graphics and computer vision.
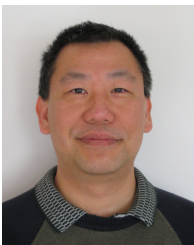
Sing Bing Kang (M'90–F'12) received his Ph.D. degree in robotics from Carnegie Mellon University, Pittsburgh, in 1994. He is Principal Researcher at Microsoft Corporation, and his research interests include image and video enhancement, and image-based modeling. He has coedited two books (Panoramic Vision and Emerging Topics in Computer Vision) and coauthored two books (Image-Based Rendering and Image-Based Modeling of Plants and Trees). On the community service front, he has served as Area Chair for the major computer vision conferences and as papers committee member for SIGGRAPH and SIGGRAPH Asia. He was Program Chair for ACCV 2007 and CVPR 2009, and was Associate Editor-In-Chief for IEEE Transactions on Pattern Analysis and Machine Intelligence from 2010-2014. He is a fellow of the IEEE.
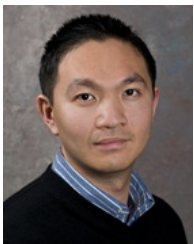
Jingyi Yu is a professor at Computer and Information Science Department at the University of Delaware. He received his B.S. from Caltech in 2000 and M.S. and Ph.D. degree in EECS from MIT in 2005. His research interests span a range of topics in computer graphics, computer vision, and image processing, including computational photography, medical imaging, nonconventional optics and camera design, tracking and surveillance, and graphics hardware.